Radial Basis Function Interpolation for Rapid Interactive Segmentation of 3-D Medical Images

Negar Mirshahzadeh[1*], Tanja Kurzendorfer[1], Peter Fischer[2], Thomas Pohl[2], Alexander Brost[2], Stefan Steidl[1], and Andreas Maier[1]

[1] Pattern Recognition Lab, FAU Erlangen-Nuremberg, Erlangen, Germany
n.mirshahzadeh@gmail.com, tanja.kurzendorfer@fau.de,
stefan.steidl@fau.de, andreas.maier@fau.de,
[2] Siemens Healthcare GmbH, Forchheim, Germany
peterfischer@siemens-healthineers.com,
thomas.tp.pohl@siemens-healthineers.com,
alexander.brost@siemens-healthineers.com

Abstract. Segmentation is one of the most important parts of medical image processing. Manual segmentation is very cumbersome and time-consuming. Fully automatic segmentation approaches require a large amount of labeled training data and may fail in difficult cases. In this paper, we propose a new method for 2-D segmentation and 3-D interpolation. The Smart Brush functionality quickly segments the ROI in a few 2-D slices. Given these annotated slices, our adapted formulation of Hermite Radial Basis Functions reconstructs the 3-D surface. Effective interactions with less number of equations accelerate the performance and therefore, a real-time and an intuitive, interactive segmentation can be supported effectively. The proposed method was evaluated on 12 clinical 3-D MRI data sets from individual patients and were compared to gold standard annotations of the left ventricle from a clinical expert. The 2-D Smart Brush resulted in an average Dice coefficient of 0.88 ± 0.09 for individual slices. For the 3-D interpolation using Hermite Radial Basis Functions an average Dice coefficient of 0.94 ± 0.02 was achieved.

Keywords: smart brush, segmentation, 3-D interpolation, HRBF

1 Introduction

A great deal of effort has gone into interactive segmentation. Many segmentation techniques have been developed such as Intelligent Scissors, Graph Cuts, and Random Walker [9,3,5]. There are two important applications that these techniques can speed up. First, manual segmentation is still widespread in clinical routine and which is arduous. Second, the training of machine learning methods for segmentations needs ground truth annotations that have to be generated manually. In particular, deep learning is known to require huge amounts of annotated data. Therefore, the challenge is to design a fast, generic and easy segmentation tool that allows to generate clinical segmentations as well as fast

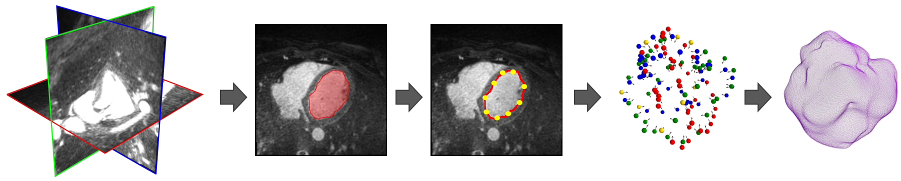

Fig. 1. Segmentation pipeline. The first image from left to right shows the 3-D volume as input. In the next step, single slices are segmented using the Smart Brush functionality. Third, the control points of the contours are extracted. Fourth, the 2-D and 3-D normal vectors are computed for the Hermite Radial Basis Function (HRBF) interpolation. In the final image, the interpolated surface is visualized.

ground truth annotations. The most related 2-D segmentation technique is a Smart Brush tool [7,10]. However, the drawback of this method is that it does not control the boundary smoothness [2].

In surface reconstruction, there is a vast literature which is mainly grouped into direct meshing and implicit approaches. Nowadays, those methods based on implicit surface reconstruction have gained more and more attention. In this approach, first a signed scalar field $f(\cdot)$ is obtained. The scalar value of this scalar field is zero at all scattered points (here control points $\boldsymbol{p}$), $f(\boldsymbol{p}) = 0$ and negative/positive for inside/outside of the surface [8]. Then, the desired surface is reconstructed by extracting the zero-level set of the mentioned field. In previous related work [6], this filed $f(\cdot)$ is computed in a bilateral domain where the spatial and intensity range domain are joined. The interpolation is done using the Radial Basis Function (RBF) with a Hermite data type which incorporates normals and gradients of the scalar field directly, $\nabla f(\boldsymbol{p}) = \boldsymbol{n}$.

In this work, we propose a new formulation of surface reconstruction which is independent of the 3-D intensity gradient information. The interpolation is mainly based on 2-D normal vectors obtained from the segmented slices in 2-D. Hence, a Smart Bush formulation is introduced which can handle medical acquisitions with higher noise level and ambiguous boundaries using a Gaussian Mixture Model (GMM). Furthermore, 3-D normal vectors are estimated for the intersections of annotated planes from different orientations. From this it follows, that the surface is reconstructed using both 2-D and 3-D normal vectors. In contrast to previous implicit methods, this combination can be applied to images with a high noise level, as it is not dependent on any intensity information or well defined borders.

2 Methods

Our approach combines advantages of semi-automatic segmentation methods as well as the user's high-level anatomical knowledge to generate segmentations quickly and accurately with fewer interactions. Using our method, the user first segments a few slices with the Smart Brush, then the scattered data points are extracted by computing the 2-D gradient information of the annotated slices. Applying our new formulation of Hermite Radial Basis Function (HRBF), the desired surface is reconstructed. In Fig. 1 the segmentation pipeline is illustrated.

2.1 Smart Brush

The 2-D segmentation functionality classifies pixels into foreground and background based on intensity. Initially, a small initial area in the foreground has to be segmented manually by the user. The mean intensity of the initial area is required for the smart brush functionality.

When the user selects a new ROI with the brush, an unsupervised GMM with two components is fitted for the ROI. A threshold for pixel-wise classification is derived as the mean of the two mixture component means. The pixels of the component whose mean is closer to the mean intensity of the initial area are classified as foreground. Finally, to reduce false positives, the morphological connectivity of each pixel in the ROI to the initial ROI is checked using a 4-connected structuring element. This way, pixels that has the same intensity value but are not connected to the previous segmentation are removed.

2.2 Control Point Extraction

We assume that multiple slices are segmented in axial, sagittal, and coronal orientation using the Smart Brush functionality. First, the contours are extracted from the segmentations. Then, control points (CPs) are computed from the contours adaptively according to the shape of the object.

The contour is sampled equidistantly with a predefined sampling size $\delta \in \mathbb{Z}$. The number of control points $n_e \in \mathbb{Z}$ is based on the contour length $l_c \in \mathbb{Z}$ and computed as $n_p = \lfloor \frac{l_c}{\delta} \rfloor$. Furthermore, $n_c \in \mathbb{Z}$ convexity defect points, where the contour has the maximum distance to its convex hull, are added. To increase the accuracy of the 3-D interpolation for complex objects, the number of CPs is increased at rough areas. Therefore, the local curvature $\kappa \in \mathbb{R}$ is checked for all CPs and additional points are added in case of roughness. To compare curvature values, a reference quantity $r \in \mathbb{R}$ (global roughness) is defined which is the ratio of the convex hull area A_h and the entire curve area A_c, $r = A_c/A_h$ [1]. New CPs are added at a certain distance to the investigated CP, if the criterion

$$\frac{\kappa}{r} \geqslant \theta_r \tag{1}$$

is fulfilled, where the threshold $\theta_r \in \mathbb{R}$ is obtained heuristically. The number of additional CPs due to curvature is denoted as n_κ. The total number of CPs is $N = n_e + n_c + n_\kappa$. Fig. 2 depicts two methods of control point extraction.

The subsequent interpolation requires Hermite data, i.e., function values and their derivatives. In this case, we need the normal vector for each control point. The first derivative of the contour approximates the tangent vector of the curve. Having the 2-D tangent vector $\boldsymbol{t} = (d_x, d_y)^T$, the orthogonal normal vector is obtained by $\boldsymbol{n} = (-d_y, d_x)^T$.

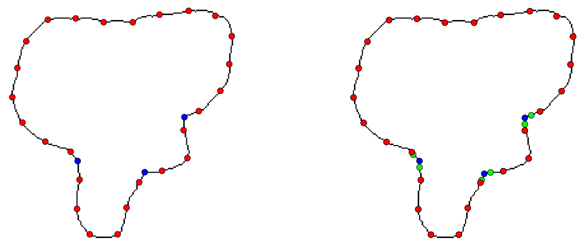

Fig. 2. (a) A rough surface with initial equidistant points in red and convexity defect points in blue. (b) A rough surface with increased number of points in green.

2.3 3-D Interpolation

A new formulation of HRBF is introduced that allows to reconstruct the 3-D surface based on scattered control points and their associated 2-D normal vectors only. Assume that N Hermite data points $\{(\boldsymbol{p}_i, \boldsymbol{n}_i) | \boldsymbol{p}_i \in \mathbb{R}^3, \boldsymbol{n}_i \in \mathbb{R}^2, i = 1, ..., N\}$ are generated from Section 2.2. In RBF interpolation, the final segmentation is given as the zero level set of a scalar field. The scalar field f is formulated as

$$f(\boldsymbol{x}) = \sum_{i=1}^{N} \alpha_i \varphi\left(\|\boldsymbol{x} - \boldsymbol{p}_i\|\right) - \boldsymbol{\beta}_i^T \cdot s_i^{\mathrm{2D}}\left(\nabla \varphi\left(\|\boldsymbol{x} - \boldsymbol{p}_i\|\right)\right) + g\left(\boldsymbol{x}\right), \tag{2}$$

where $g(\boldsymbol{x})$ is a low-degree polynomial, $s_i^{\mathrm{2D}}(\boldsymbol{x})$ is a function that selects the 2-D gradient direction that is available for control point i, and the RBF coefficients $\alpha_i \in \mathbb{R}$, $\boldsymbol{\beta}_i \in \mathbb{R}^2$. According to previous work [6], the commonly used tri-harmonic kernel $\varphi(t) = t^3$ with a linear polynomial $g(\boldsymbol{x}) = \boldsymbol{a}^T\boldsymbol{x} + b$ yields adequate results in terms of shape aesthetics. To determine the coefficients α_i and $\boldsymbol{\beta}_i$, constraints are derived from the CPs [6]

$$f\left(\boldsymbol{p}_i\right) = 0 \tag{3}$$

$$s_i^{\mathrm{2D}}\left(\nabla f\left(\boldsymbol{p}_i\right)\right) = \boldsymbol{n}_i \ . \tag{4}$$

In addition, the orthogonality conditions $\sum_{i=1}^{N} \alpha_i = 0$ and $\sum_{i=1}^{N} \alpha_i s_i^{\mathrm{2D}}(\boldsymbol{p}_i) + \boldsymbol{\beta}_i = \boldsymbol{0}$ have to be fulfilled. This yields a linear system of equations of $3(N+1) \cdot 3(N+1)$ order which can be denoted with a block form as

$$\begin{pmatrix} \boldsymbol{0} & \boldsymbol{S}_1^T & \cdots & \boldsymbol{S}_N^T \\ \boldsymbol{S}_1 & \boldsymbol{K}_{1,1} & \cdots & \boldsymbol{K}_{1,N} \\ \vdots & \vdots & \ddots & \vdots \\ \boldsymbol{S}_N & \boldsymbol{K}_{N,1} & \cdots & \boldsymbol{K}_{N,N} \end{pmatrix} \begin{pmatrix} \boldsymbol{s} \\ \boldsymbol{w}_1 \\ \vdots \\ \boldsymbol{w}_N \end{pmatrix} = \begin{pmatrix} \boldsymbol{0} \\ \boldsymbol{c}_1 \\ \vdots \\ \boldsymbol{c}_N \end{pmatrix}, \tag{5}$$

where for CPs with Hermite data based on 2-D normals, the blocks $\boldsymbol{K}_{i,j}$, $\boldsymbol{S}_i \in \mathbb{R}^{3\times 3}$ and vectors $\boldsymbol{s}$, $\boldsymbol{w}_i$ and $\boldsymbol{c}_i$ are defined as:

$$\begin{gathered}\boldsymbol{K}_{i,j} = \begin{pmatrix} \varphi(\|\boldsymbol{p}_i - \boldsymbol{p}_j\|) & -s_i^{2D}\left(\nabla\varphi(\|\boldsymbol{p}_i - \boldsymbol{p}_j\|)\right)^T \\ s_i^{2D}\left(\nabla\varphi(\|\boldsymbol{p}_i - \boldsymbol{p}_j\|)\right) & -\nabla^T s_i^{2D}\left(\nabla\varphi(\|\boldsymbol{p}_i - \boldsymbol{p}_j\|)\right) \end{pmatrix}, \\ \boldsymbol{S}_i = \begin{pmatrix} s_i^{2D}(\boldsymbol{p}_i)^T & 1 \\ \boldsymbol{I} & \boldsymbol{0} \end{pmatrix}, \quad \boldsymbol{s} = \begin{pmatrix} \boldsymbol{a} \\ b \end{pmatrix}, \quad \boldsymbol{w}_i = \begin{pmatrix} \alpha_i \\ \boldsymbol{\beta}_i \end{pmatrix}, \quad \boldsymbol{c}_i = \begin{pmatrix} \boldsymbol{0} \\ \boldsymbol{n}_i \end{pmatrix},\end{gathered} \tag{6}$$

where $\boldsymbol{I} \in \mathbb{R}^{2\times 2}$ is the identity matrix and $\nabla^T s_i^{2D}(\nabla \boldsymbol{x}) \in \mathbb{R}^{2\times 2}$ is the Hessian of the available 2-D dimensions. There is always a unique solution to the system of equations if the points $\boldsymbol{p}_i$ are pairwise distinct [4,6]. The unknown parameters $\alpha_i, \boldsymbol{\beta}_i, \boldsymbol{a}$ and b can be obtained directly as the matrix is square and non-singular.

However, through the segmentation of several slices from different orientations, control points can be close together at the intersection of the planes. The normal vectors of these points, point in a different direction according to the segmented contour. To make the interpolation result even more robust, these points are combined and a 3-D normal vector is estimated. The merging is performed with in a certain user defined radius around each intersection area. Hence, the HRBF interpolation is a combination of 2-D and 3-D normal vectors. Assuming N CPs with 2-D normals and M CPs with 3-D normal, the extended system of equations is

$$\begin{pmatrix} \boldsymbol{0} & \boldsymbol{S}_1^T & \cdots & \boldsymbol{S}_M^T & \boldsymbol{S}_{M+1}^T & \cdots & \boldsymbol{S}_{M+N}^T \\ \boldsymbol{S}_1 & \boldsymbol{K}_{1,1} & \cdots & \boldsymbol{K}_{1,M} & \boldsymbol{K}_{1,M+1} & \cdots & \boldsymbol{K}_{1,M+N} \\ \vdots & \vdots & \ddots & \vdots & \vdots & \ddots & \vdots \\ \boldsymbol{S}_M & \boldsymbol{K}_{M,1} & \cdots & \boldsymbol{K}_{M,M} & \boldsymbol{K}_{M,M+1} & \cdots & \boldsymbol{K}_{M,M+N} \\ \boldsymbol{S}_{M+1} & \boldsymbol{K}_{M+1,1} & \cdots & \boldsymbol{K}_{M+1,M} & \boldsymbol{K}_{M+1,M+1} & \cdots & \boldsymbol{K}_{M+1,M+N} \\ \vdots & \vdots & \ddots & \vdots & \vdots & \ddots & \vdots \\ \boldsymbol{S}_{M+N} & \boldsymbol{K}_{M+N,1} & \cdots & \boldsymbol{K}_{M+N,M} & \boldsymbol{K}_{M+N,M+1} & \cdots & \boldsymbol{K}_{M+N,M+N} \end{pmatrix} \begin{pmatrix} \boldsymbol{s} \\ \boldsymbol{w}_1 \\ \vdots \\ \boldsymbol{w}_M \\ \boldsymbol{w}_{M+1} \\ \vdots \\ \boldsymbol{w}_{M+N} \end{pmatrix} = \begin{pmatrix} \boldsymbol{0} \\ \boldsymbol{c}_1 \\ \vdots \\ \boldsymbol{c}_M \\ \boldsymbol{c}_{M+1} \\ \vdots \\ \boldsymbol{c}_{M+N} \end{pmatrix}, \tag{7}$$

where different color in the matrix implies the points and the corresponding normal vectors with different dimensionality (3-D blue, 2-D green, mixed purple).

3 Evaluation and Results

The evaluation was performed on 12 MRI data sets. Gold standard annotations of the left ventricle were provided by a clinical expert. The Dice coefficient was evaluated as a quantitative score for the segmentation overlap. The 2-D ground truth annotation was used to assess the 2-D segmentation and the complete 3-D ground truth for the 3-D interpolation scheme. The main problem with evaluating the Smart Brush is that it inherently involves human interaction. Therefore, objective testing without human interaction is difficult. To address this, we mimicked user interactions such as slice selection, mouse movement, brush size, etc. Iteratively, a 2-D slice was selected and one patch of the ground truth was used for training. The evaluation of the Smart Brush was performed on a different patch by computing the Dice coefficient per patch. For evaluation of

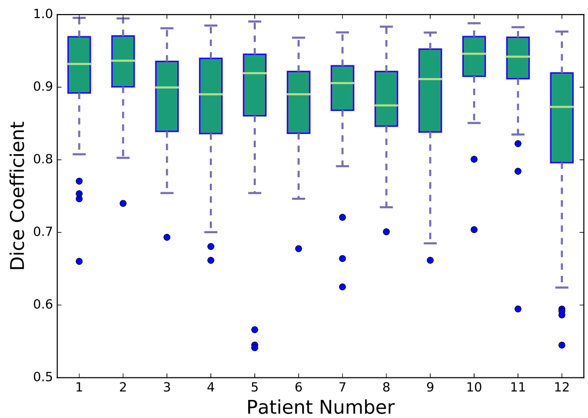

Fig. 3. The evaluation results of the 2-D segmentation result using the Smart Brush.

the 3-D interpolation, we compare our method (A-HRBF) to a reference method that extracts 3D gradients on the control points based on intensity (HRBF) [6].

The results of the 2-D evaluation of our Smart Brush are depicted in Fig. 3. For most patients, an average Dice coefficient of around 0.9 is achieved. The results of the 3-D segmentation are depicted in Fig. 4. For each data set, the evaluation was performed with a different number of segmented slices per orientation. We evaluated 1, 3, and 5 slices per orientation which means to have a total number of 3, 9, and 15 slices, respectively. The slice selection was randomly. The same method of control point extraction was used for control point computation. It can be seen that by increasing the number of slices the Dice coefficient usually increases slightly. Comparing the different methods, the Dice coefficient for the proposed A-HRBF is consistently higher than for HRBF.

Our experiments showed that three slices per orientation is sufficient to get a good segmentation result. Furthermore, in order to achieve more accurate interpolation results, the user has to segment those slices which have the maximum mismatch with the actual ground truth. In fact, for 3-D interpolation, the user selects those slices which are a good representation of the complete volume. Hence, the actual result of the interpolation is even better than the evaluation result shows. Fig. 5 depicts the qualitative results of the A-HRBF 3-D interpolation scheme for one data set.

4 Discussion and Conclusion

In contrast to previous implicit methods for 3-D interpolation [6], this method can not only be used for high-contrast images, but also for images with high noise level or other confounding factors due to the independence of intensity information. The main advantage happens when there is an ambiguous boundary

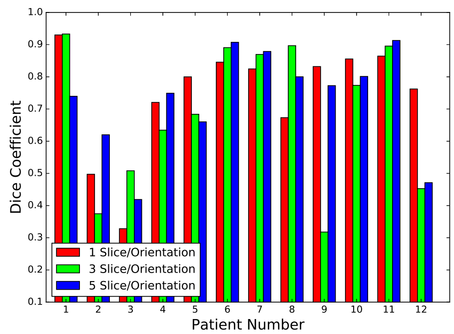

(a) HRBF

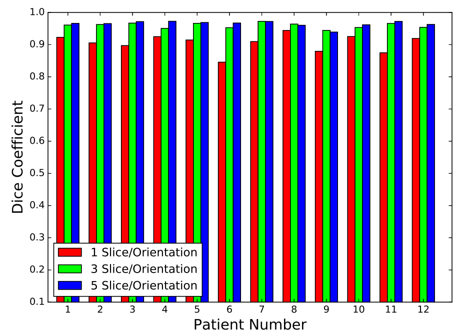

(b) A-HRBF

Fig. 4. The 3-D interpolation evaluation results: (a) The HRBF result with average Dice coefficient of 0.69, 0.63 and 0.69 for 1, 3, and 5 slice per orientation,respectively. (b) The A-HRBF result with average Dice coefficient of 0.91, 0.95 and 0.96 for 1, 3, and 5 slice per orientation, respectively.

which only an expert can recognize (e.g. between left ventricle and left atrium). In this case, normal vector computation fails based on the previous method [6], while using our method, the normal vectors are orienting properly, see Fig. 6.

We showed that the 3-D interpolation is already quite good with one slice per orientation. However, this was only evaluated for the left ventricle, which is a convex object. Considering more complex objects more annotations would be necessary.

The benefit of the method is that the user can correct the segmentation result easily by segmenting an additional slice with the maximum mismatch. Furthermore, no prior knowledge is involved which leads to the ability to generate any arbitrary segmentation of any 3-D data set, irrespective of image modality, displayed organ, or clinical application.

Disclaimer: The methods and information presented in this paper are based on research and are not commercially available.

References

1. Abbena, E., Salamon, S., Gray, A.: Modern differential geometry of curves and surfaces with Mathematica. CRC press (2006)
2. Boykov, Y., Kolmogorov, V.: Computing geodesics and minimal surfaces via graph cuts. In: ICCV. vol. 3, pp. 26–33 (2003)
3. Boykov, Y., Veksler, O., Zabih, R.: Fast approximate energy minimization via graph cuts. IEEE Trans. Pattern Anal. Mach. Intell. 23(11), 1222–1239 (2001)
4. Brazil, E.V., Macedo, I., Sousa, M.C., de Figueiredo, L.H., Velho, L.: Sketching variational hermite-rbf implicits. In: Proceedings of the Seventh Sketch-Based Interfaces and Modeling Symposium. pp. 1–8. Eurographics Association (2010)

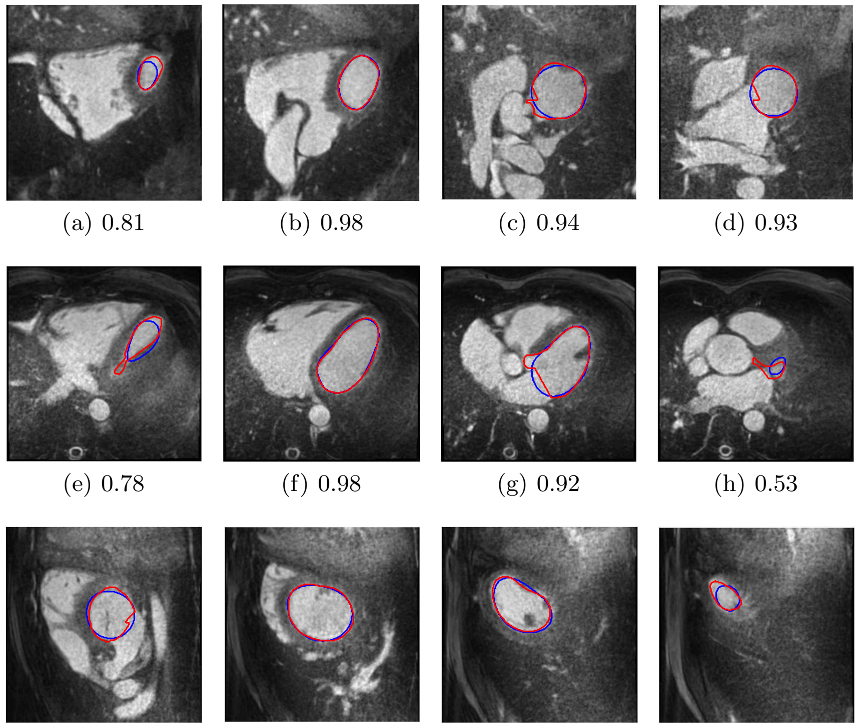

(a) 0.81 (b) 0.98 (c) 0.94 (d) 0.93

(e) 0.78 (f) 0.98 (g) 0.92 (h) 0.53

(i) 0.91 (j) 0.97 (k) 0.94 (l) 0.83

Fig. 5. The ground truth (red) and the result of 3-D interpolation (blue) are shown. The interpolation is obtained based on only one reference slice per orientation. Each row depicts a different orientation (axial, sagittal, and coronal), where the caption is the 2-D Dice coefficient of the respective slice. It is expected that the closer to the reference slice, the higher Dice coefficient is obtained.

5. Grady, L.: Random walks for image segmentation. IEEE Trans. Pattern Anal. Mach. Intell. 28(11), 1768–1783 (2006)
6. Ijiri, T., Yoshizawa, S., Sato, Y., Ito, M., Yokota, H.: Bilateral hermite radial basis functions for contour-based volume segmentation. In: Computer Graphics Forum. vol. 32, pp. 123–132. Wiley Online Library (2013)
7. Malmberg, F., Strand, R., Kullberg, J., Nordenskjöld, R., Bengtsson, E.: Smart paint a new interactive segmentation method applied to mr prostate segmentation. MICCAI Grand Challenge: Prostate MR Image Segmentation 2012 (2012)
8. Morse, B.S., Yoo, T.S., Rheingans, P., Chen, D.T., Subramanian, K.R.: Interpolating implicit surfaces from scattered surface data using compactly supported radial basis functions. In: ACM SIGGRAPH 2005 Courses. p. 78. ACM (2005)
9. Mortensen, E.N., Barrett, W.A.: Interactive segmentation with intelligent scissors. Graph. Models Image Process. 60(5), 349–384 (1998)
10. Parascandolo, P., Cesario, L., Vosilla, L., Pitikakis, M., Viano, G.: Smart brush: a real time segmentation tool for 3d medical images. In: Image and Signal Processing

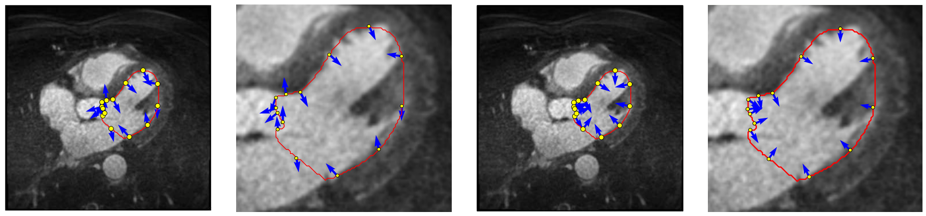

(a) (b) (c) (d)

Fig. 6. Normal vector orientation for left ventricle segmentation with an ambiguous boundary: (a,b) Control points (yellow) and associated normal vector (blue) based on intensity gradients for the HRBF method. (c,d) Control points (yellow) and associated normal vector (blue) based on the drawn contour (red) for our proposed method.

and Analysis (ISPA), 2013 8th International Symposium on. pp. 689–694. IEEE (2013)